**iScience, Volume *25***

## Supplemental information

# A collision-free gallop-based triboelectric-piezoelectric hybrid nanogenerator

**Weizhe Wang, Wei Tang, and Zhaohui Yao**

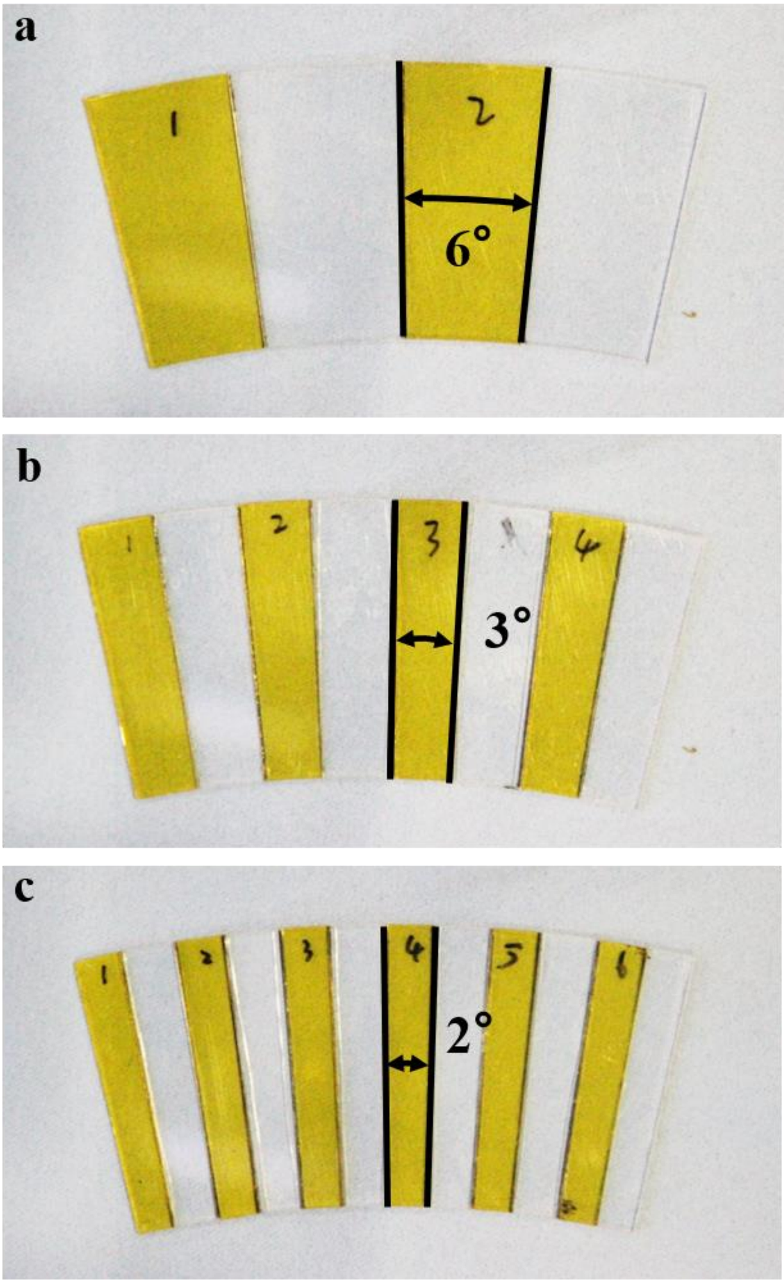


Figure. S1. Schematic diagram of acrylic plate with FEP (a) 6-degrees, (b) 3-degrees, (c) 2-degrees, Related to Figure 1.

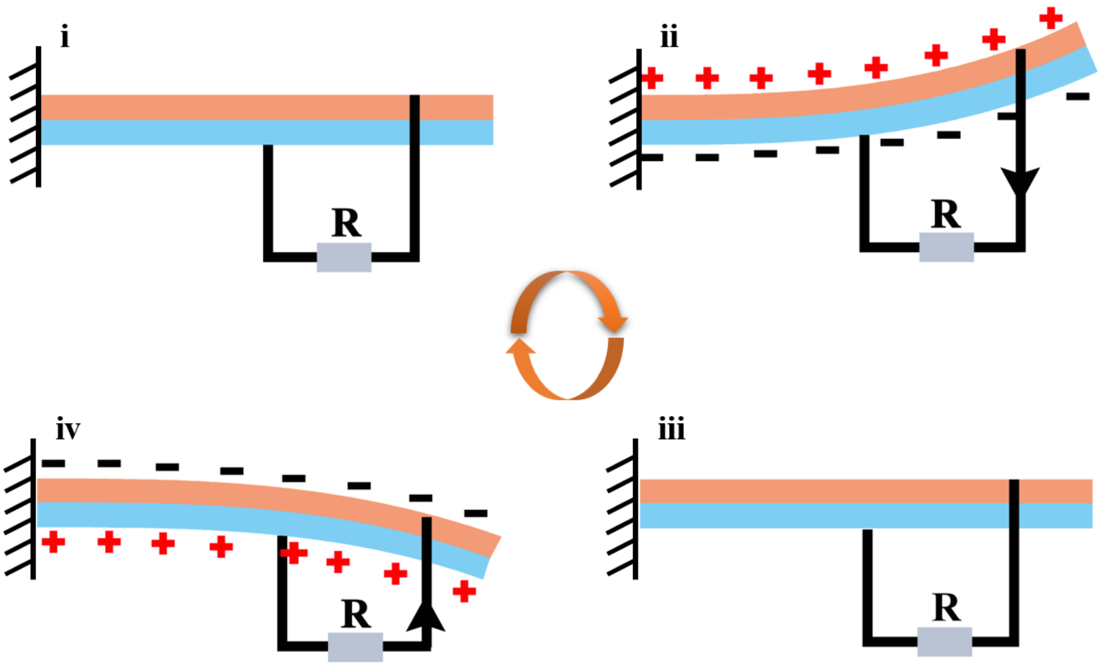


Figure. S2. Schematic diagram for the working principle of piezoelectric effect, Related to Figure 1.

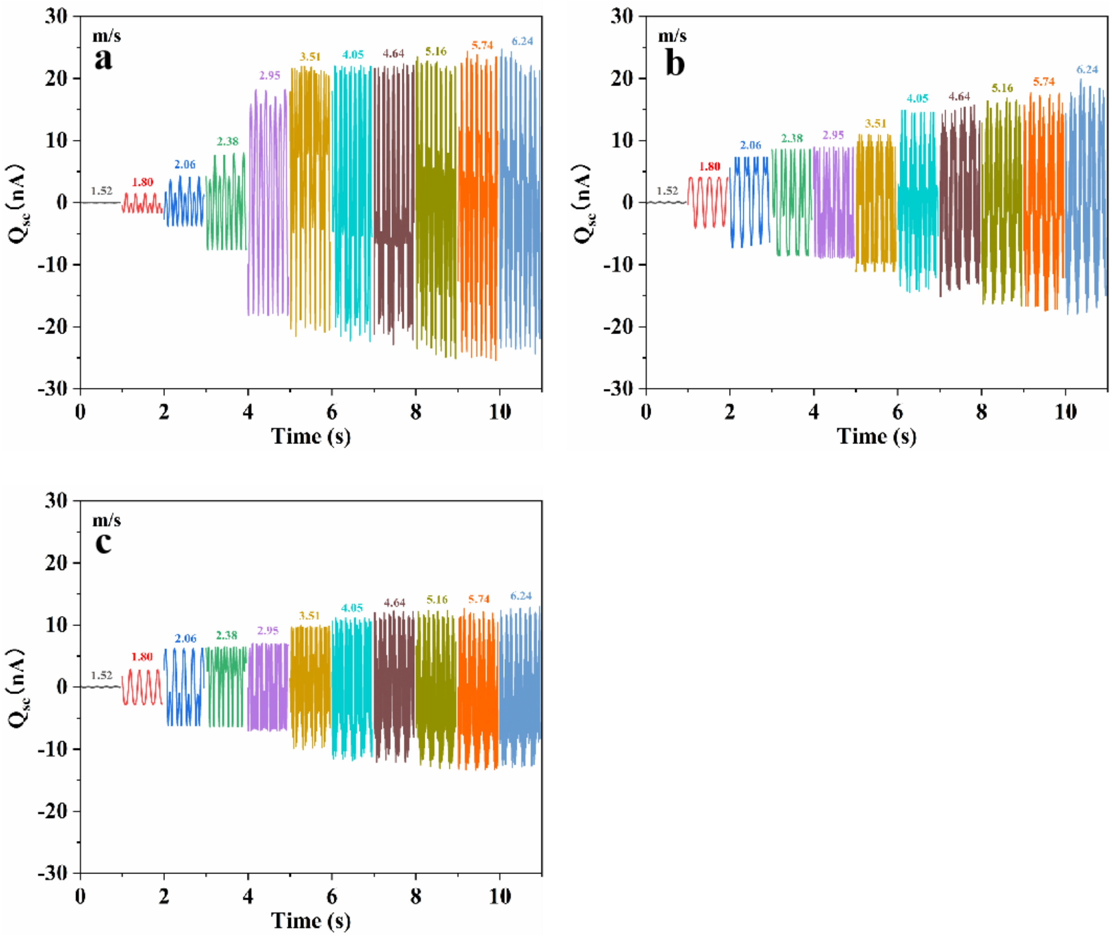


Figure. S3. Transfer charge of (a) 6-degrees, (b) 3-degrees and (c) 2-degrees G-TENG, Related to Figure 2.

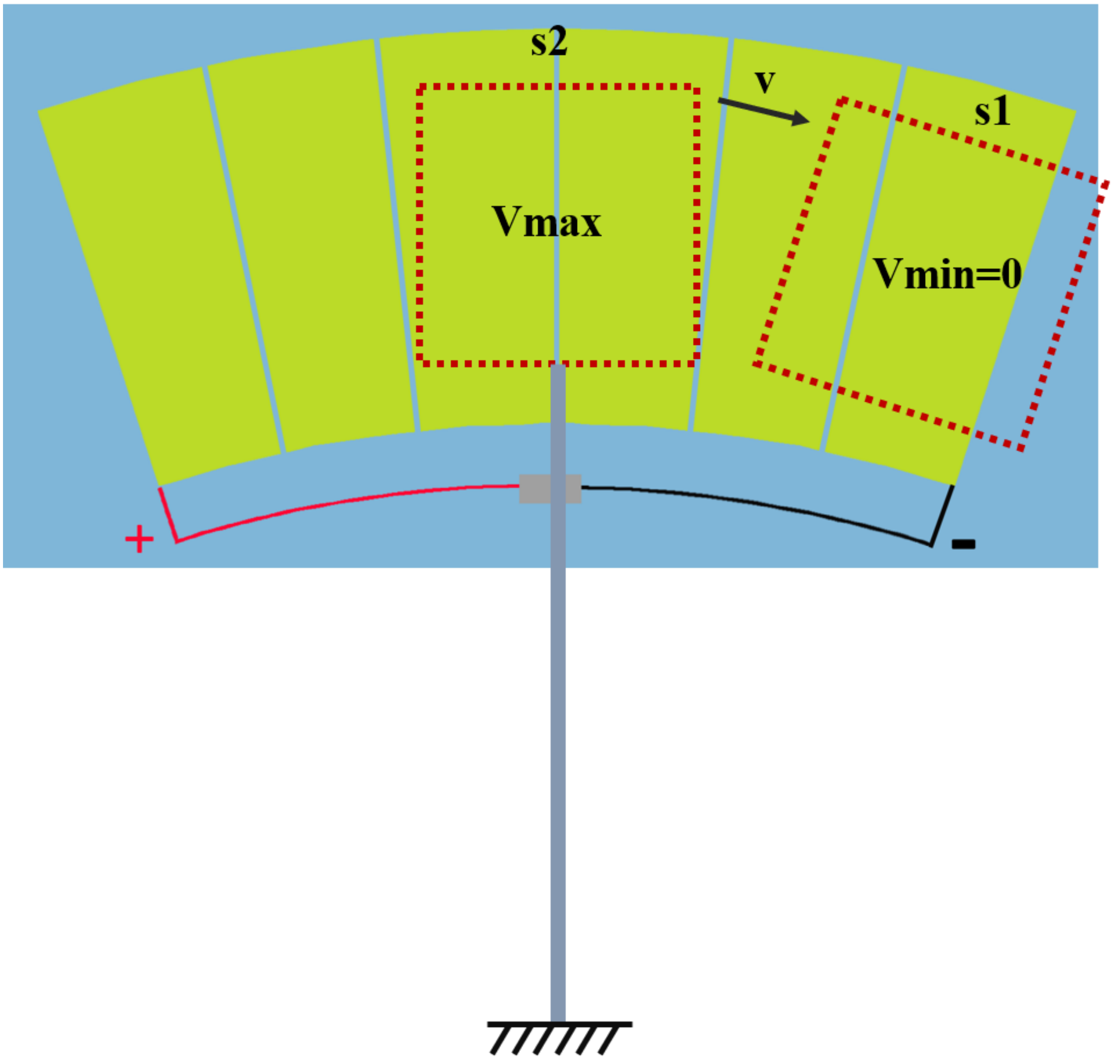


Figure. S4. Schematic diagram of the velocity of the prism motion, Related to Figure 2.

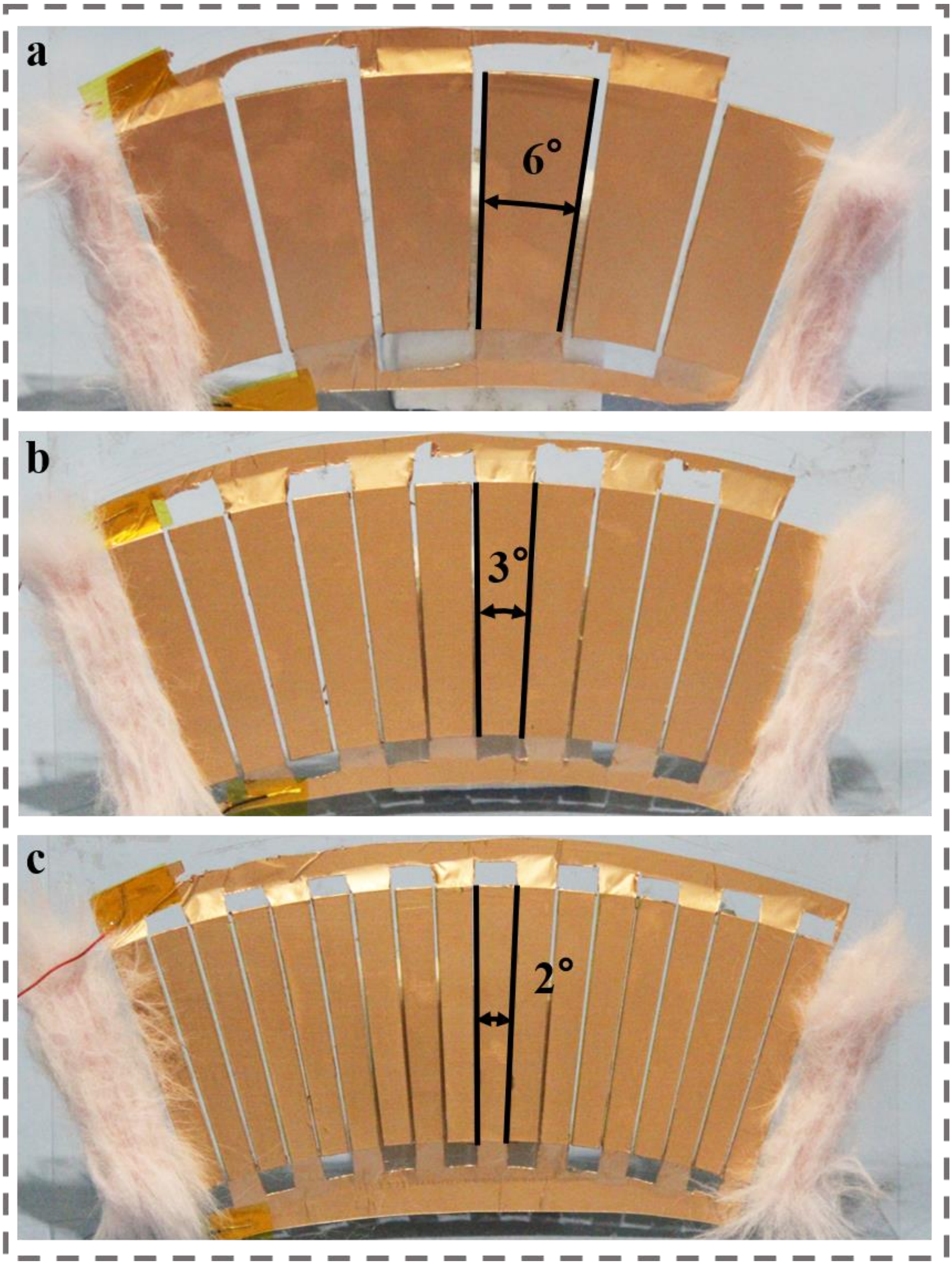


Figure. S5. Schematic diagram of the 3 types of electrodes: (a)6-degrees, (b) 3-degrees, (c) 2-degrees G-TENG, Related to Figure 2.

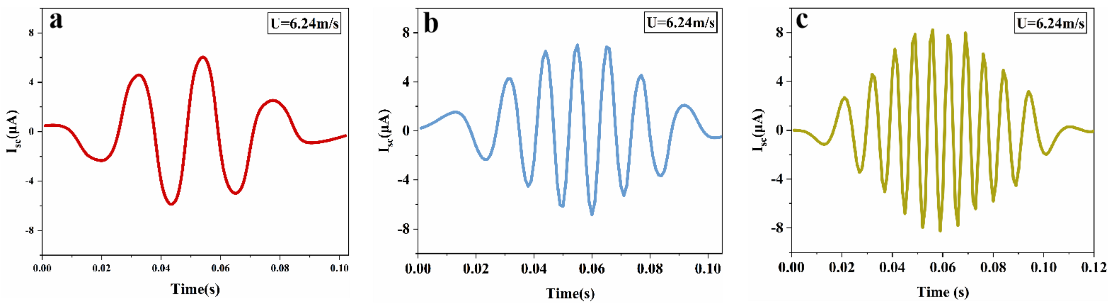


Figure.S6. Current scale-up for (a)6-degrees, (b)3-degrees, and (c)2-degrees G-TENG at wind speed of 6.24m/s, Related to Figure 2.

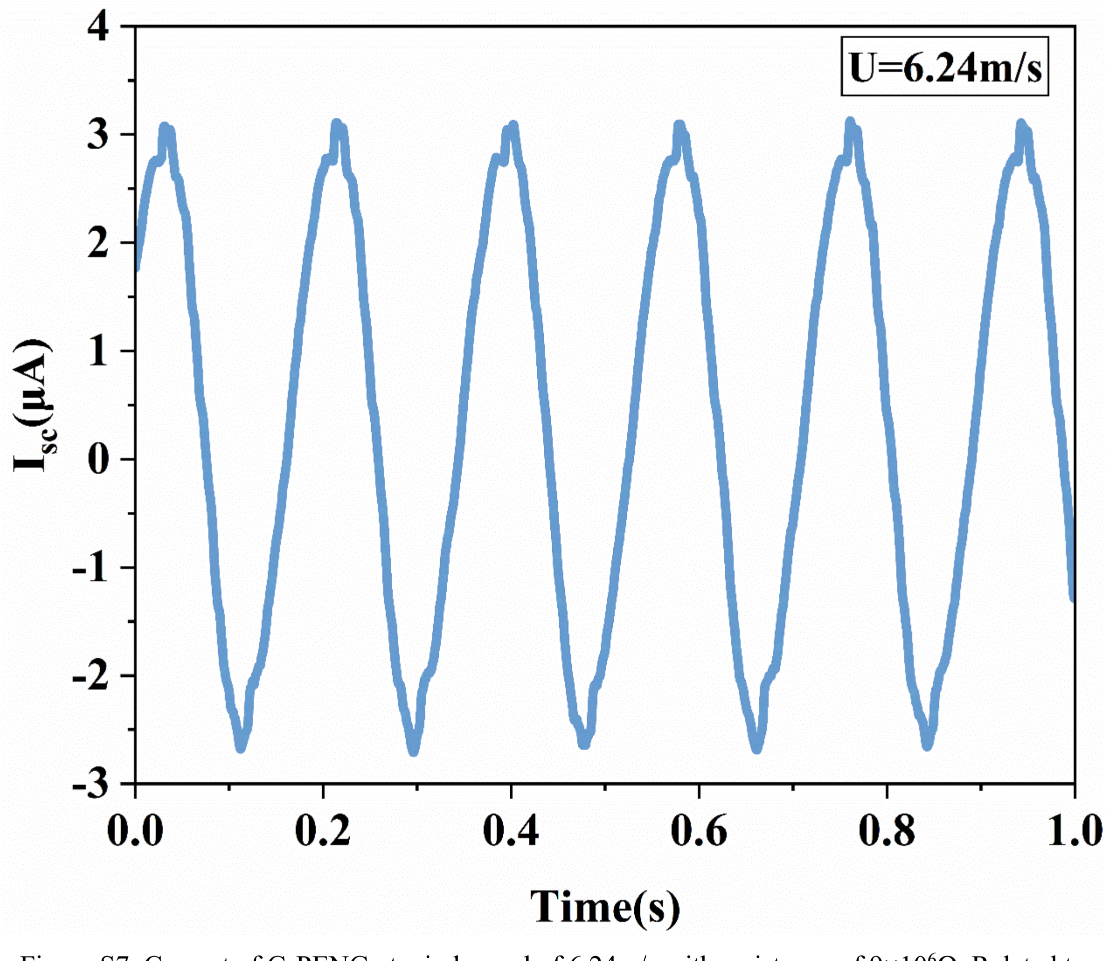


Figure.S7. Current of G-PENG at wind speed of 6.24m/s with resistance of $9\times10^{6}\Omega$, Related to Figure 2.

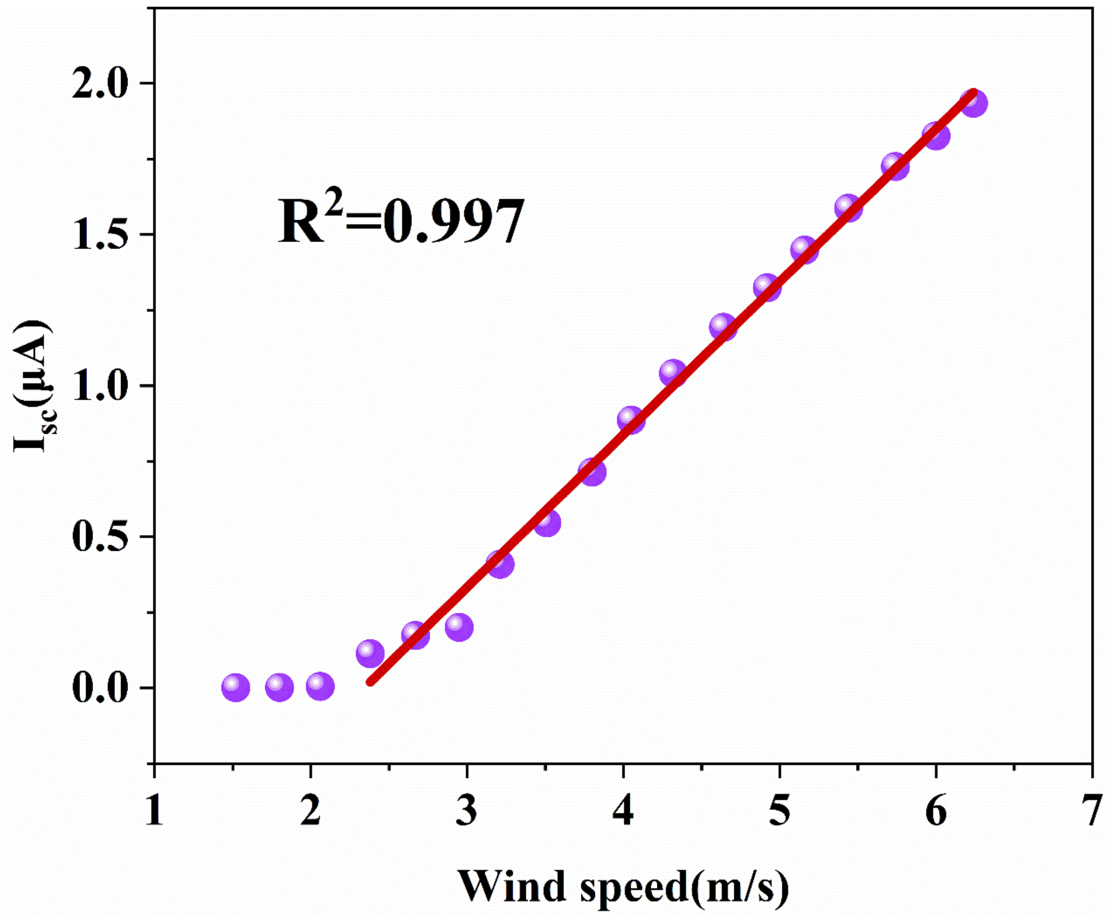

Figure.S8. Variation of the RMS current of G-PENG with wind speed, Related to Figure 2.

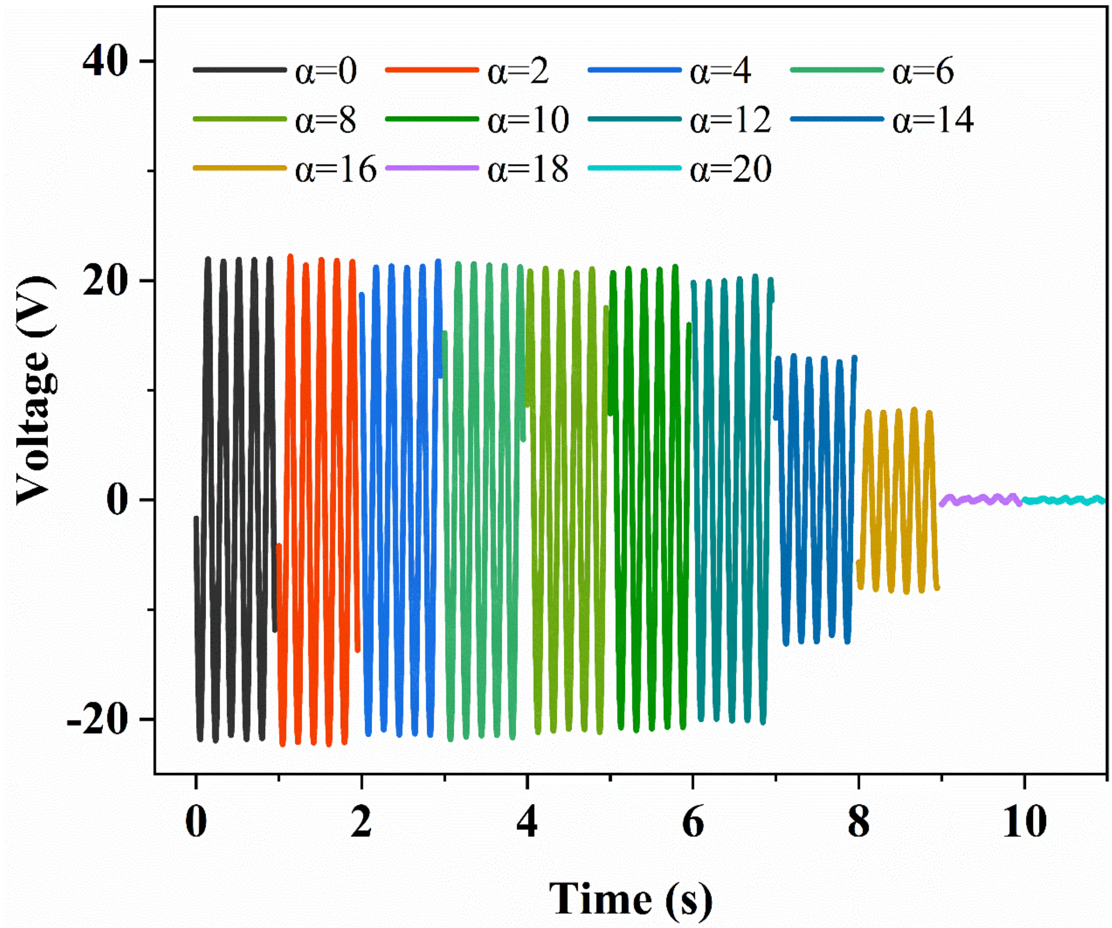


Figure. S9. Voltage variation of G-PENG with attack angle (α) at a wind speed of 6.24m/s, Related to Figure 2.

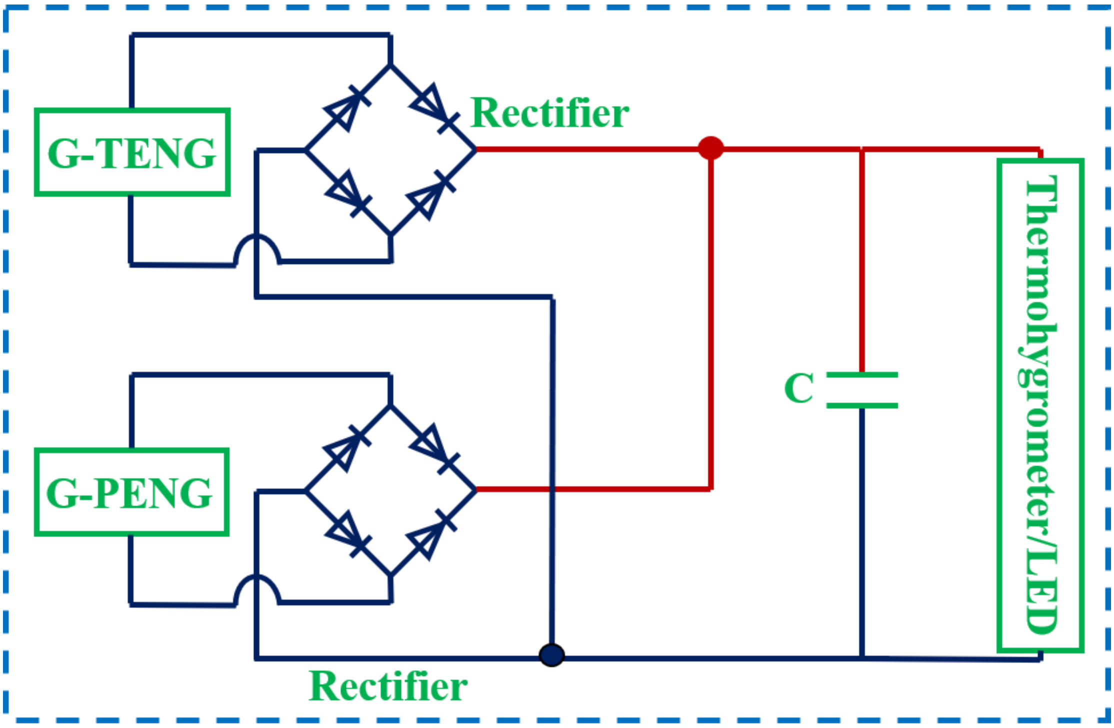

Figure. S10. Circuit diagram of HG P-TENG, Related to Figure 4.

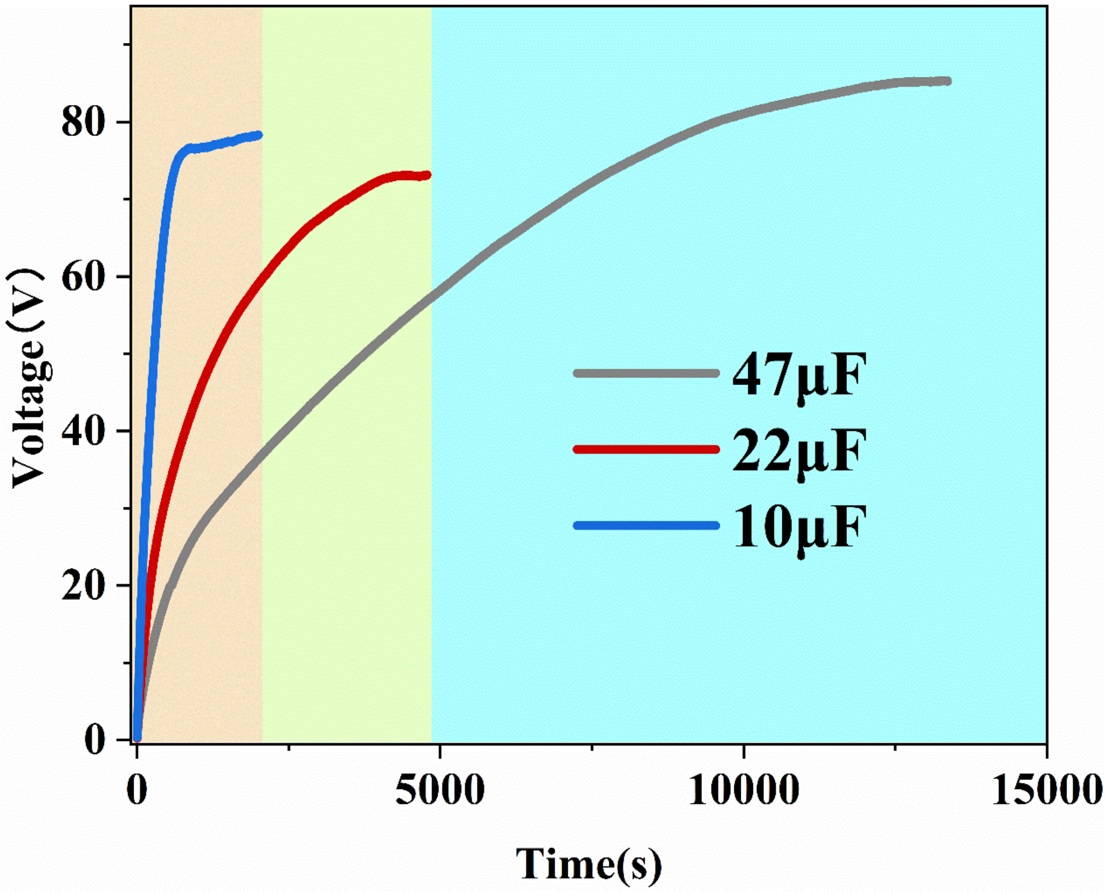


Figure. S11. Charging diagram of saturation voltage of various capacitors (3-degrees), Related to Figure 3.

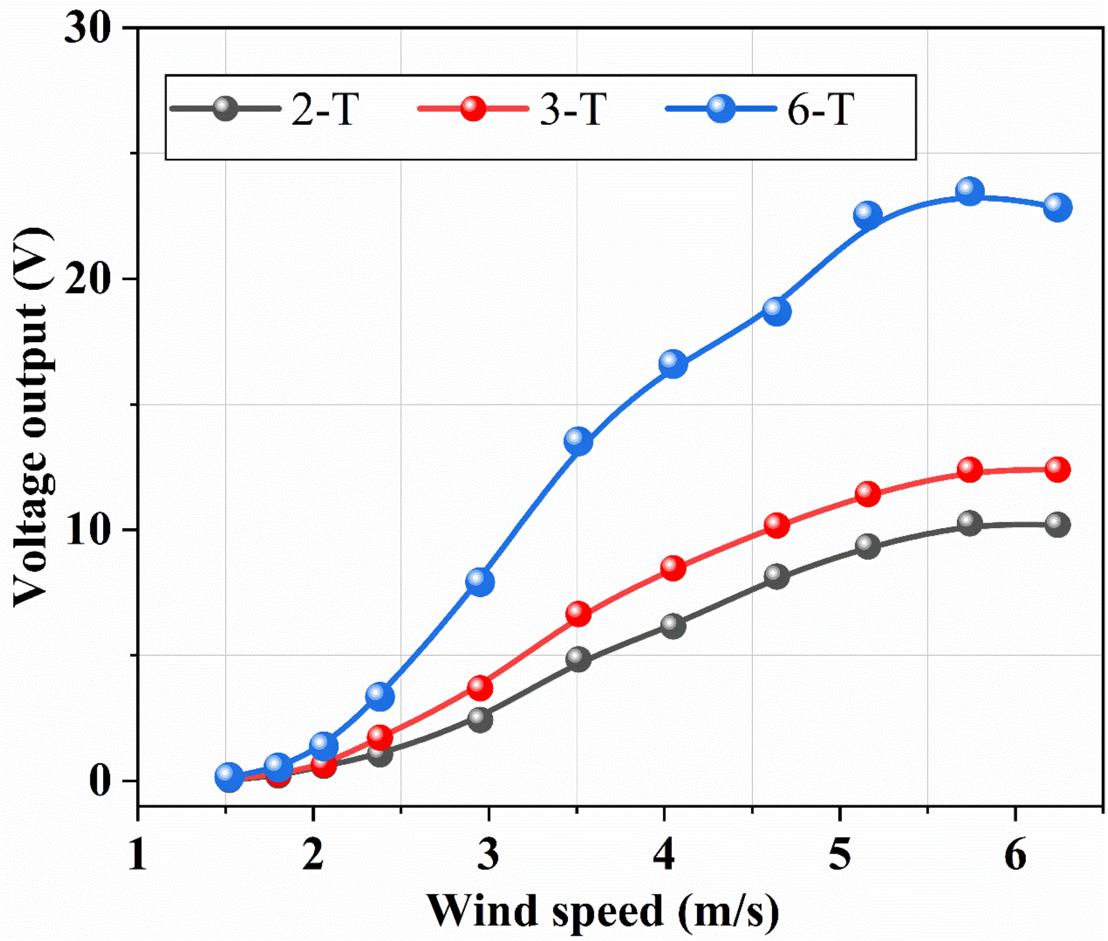

Figure.S12. RMS voltage of the 6-degrees, 3-degrees, 2-degrees G-TENG variation with wind speed, Related to Figure 4.

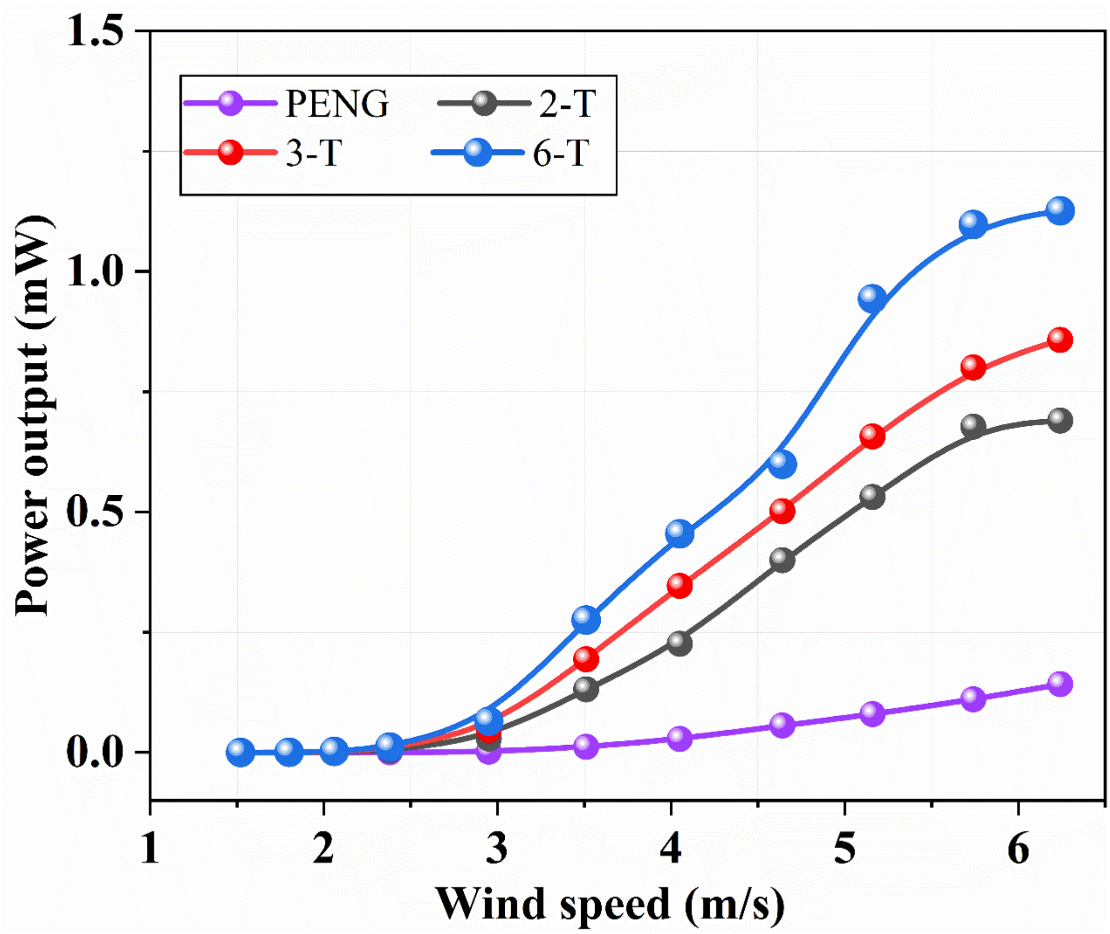


Figure.S13. The peak power of 6-degrees, 3-degrees, 2-degrees G-TENG and G-PENG variation with wind speed, Related to Figure 4.

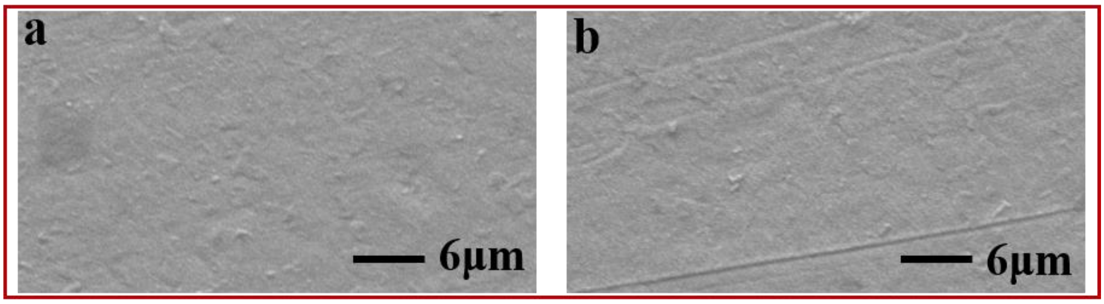


Figure.S14. Comparison of SEM images of FEP material (a) before and (b) after friction, Related to Figure 1.

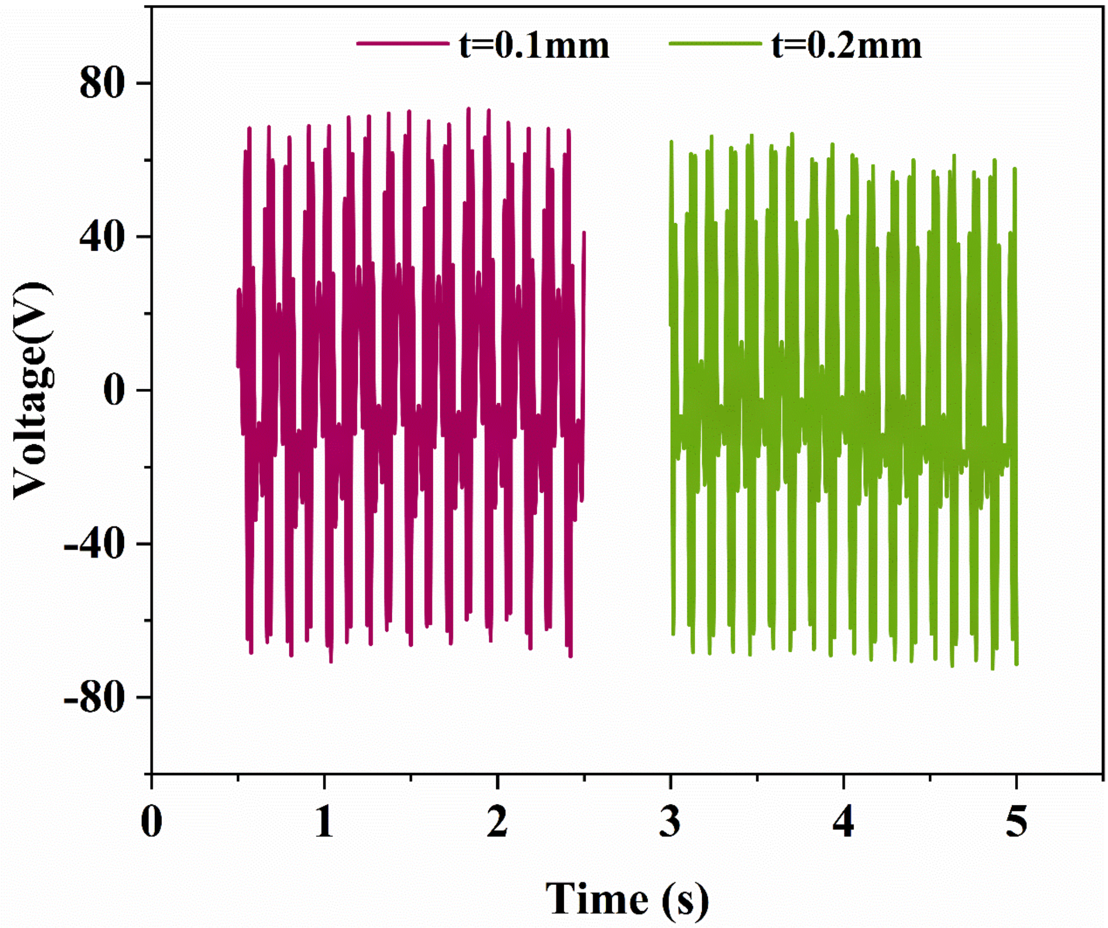


Figure. S15. Comparison of voltages for two different film thicknesses, Related to Figure 1.

Table. S1 Comparison of the advantages and disadvantages of various nanogenerators, Related to Figure 1.

| References | Working mechanism | Advantages | Disadvantages |
|---|---|---|---|
| (He et al., 2022b) | Pyroelectric | No contact required, low cost | Requires large temperature fluctuations |
| (Tashiro et al., 2002) | Electrostatic | Excellent integration with MEMS | Requires pre-powered |
| (Huang et al., 2021; Wang et al., 2020) | Piezoelectric | High energy density, miniaturization | PZT, piezoelectric fibers, and so on are overly crisp and easily damaged |
| (He et al., 2022a) | Electromagnetic | High power output and simple structure | Not suitable for harvesting low frequency energy |
| (He et al., 2022a) | Triboelectric | Low cost, easy to produce, and high voltage | Significant performance degradation in wet conditions |

Table.S2 Comparison of charging times to 5V for 10μF capacitors for similar reported energy harvesters, Related to Figure 3.

| Number | Charing time | Output power | References |
|---|---|---|---|
| 1 | Much greater than 100s | Average 10μW | (Hu et al., 2019) |
| 2 | About 100s | $20mW/m^2$ | (Li et al., 2022) |
| 3 | About 76s | 1.04mW | (Lu et al., 2021) |
| 4 | About 70s | 4 mW | (Wu et al., 2014) |
| 5 | About 52s | 1.3 mW | (Zeng et al., 2020) |
| 6 | About 16s | 2.81 mW | (L. Zhang et al., 2020) |
| 7 | About 11s | 4.65 mW | (Y. Zhang et al., 2020) |
| 8 | About 11s | 1.27 mW | present work |
| 9 | About 94s (47μF) | Average 1.76mW | (Ye et al., 2021) |
| 10 | About 39s (47μF) | 1.27 mW | present work |